

Ising and Potts Models on Quenched Random Gravity Graphs

Wolfhard Janke¹ and Desmond A. Johnston²

¹ Institut für Theoretische Physik, Universität Leipzig
D-04109 Leipzig, Germany

² Department of Mathematics, Heriot-Watt University
Edinburgh, EH14 4AS, Scotland

Abstract

We report on single-cluster Monte Carlo simulations of the Ising, 4-state Potts and 10-state Potts models on quenched ensembles of planar, tri-valent (Φ^3) random graphs. We confirm that the first-order phase transition of the 10-state Potts model on regular 2D lattices is softened by the quenched connectivity disorder represented by the random graphs and that the exponents of the Ising and 4-state Potts models are altered from their regular lattice counterparts. The behaviour of spin models on such graphs is thus more analogous to models with quenched bond disorder than to Poissonian random lattices, where regular lattice critical behaviour persists.

Using a wide variety of estimators we measure the critical exponents for all three models, and compare the exponents with predictions derived from taking a quenched limit in the KPZ formula for the Ising and 4-state Potts models. Earlier simulations suggested that the measured values for the 10-state Potts model were very close to the predicted quenched exponents of the *four*-state Potts models. The analysis here, which employs a much greater range of estimators and also benefits from greatly improved statistics, still supports these numerical values.

1 Introduction

There has recently been some interest, and no little controversy, regarding the critical behaviour of systems with quenched bond disorder in 2D [1]. It has been known for some time that the first-order phase transition displayed by $q > 4$ -state Potts models on regular lattices is softened by the introduction of the quenched bond disorder to a continuous transition [2], though the universality class of this transition and its dependence on the strength and nature of the bond disorder are still not completely clear [3, 4]. Models which already display a continuous transition in the pure case appear to have their critical exponents altered by the bond disorder [5, 6, 7] provided that the critical exponent α_{pure} of the specific heat is positive. In addition, a qualitatively new phenomenon in the form of multi-fractal scaling of local correlators has also been predicted [8] and measured [9] when quenched bond disorder is present. It should be remarked that all of the theoretical results in the bond disordered case are perturbative in nature, which is in large measure the source of the controversy surrounding the various predictions for critical exponents, since the domain of validity is unclear.

Another type of disorder that might be imposed is quenched *connectivity* disorder. Very high accuracy numerical simulations have shown that spin models on Poissonian random lattices in both 2D [10] and 3D [11] stay stubbornly identical to their regular lattice brethren - there is no sign of the effects observed with quenched bond disorder. However, a different picture emerges when one considers spin models living on a quenched ensemble of tri-valent (Φ^3) planar graphs, as generated by simulations of 2D quantum gravity. In this case the connectivity disorder is sufficiently strong for $q > 4$ Potts model transitions to be softened to continuous transitions [12] and for $q \leq 4$ exponents to be modified from their regular 2D lattice values [13]. In this respect such planar random graphs appear to be much more akin to random bond disorder models than to the Poissonian random lattices considered in [10, 11]. One very interesting feature of the Φ^3 graphs is that exact, rather than perturbative, predictions for exponents exist in the $q \leq 4$ case, by virtue of taking a quenched limit [8, 14] in the KPZ formula which gives the weights of conformal operators when they are coupled to 2D quantum gravity.

In the quantum gravity and string theory context one is typically interested in *annealed* rather than quenched connectivity disorder, in which the lattices and spins are interacting on the same time scale, providing a discrete analogue of the back reaction in continuum theories of gravity. In this case the relation between the bare (Δ) and dressed ($\tilde{\Delta}$) weights is given by the KPZ relation [15]

$$\tilde{\Delta} = \frac{\sqrt{1-c+24\Delta} - \sqrt{1-c}}{\sqrt{25-c} - \sqrt{1-c}}. \quad (1)$$

In order to calculate the dressed weights in the quenched case one should take $c = 0$ in the KPZ relation to get

$$\tilde{\Delta}_{\text{quenched}} = \frac{\sqrt{1+24\Delta} - 1}{4}, \quad (2)$$

which now gives non-rational weights. Indeed, Cardy [8] has recently pointed out that the n th power of a correlator with bare weight Δ averaged over the disorder will scale not as $n\tilde{\Delta}$, but rather

$$\tilde{\Delta}_n = \frac{\sqrt{1+24n\Delta} - 1}{4}, \quad (3)$$

with a “typical” ¹ value being governed by [8]

$$\left. \frac{\partial \tilde{\Delta}_n}{\partial n} \right|_{n=0} = 3\Delta. \quad (4)$$

In this paper we concern ourselves exclusively with measuring quantities which correspond to $n = 1$ in the formula above, such as the specific heat, susceptibility and magnetisation. The picture suggested by the earlier $q = 2$ and $q = 10$ simulations in [12, 13] was that measurements were in accordance with the predicted quenched exponents for $q \leq 4$ and that the exponents of the quenched $q > 4$ models were “stuck” at the $q = 4$ values, as evinced by the good agreement between the measured $q = 10$ exponents and the quenched $q = 4$ predictions. This was somewhat similar to the original scenario postulated for the quenched bond disordered Potts models, where it was suggested that all bond disordered $q > 4$ Potts models displayed Ising-like criticality. An obvious test of the scenario for quenched connectivity disorder is to perform simulations at $q = 4$, as well as improving the quality of the measurements for $q = 2$ and $q = 10$ in order to get sharper estimates of the exponents in these cases. This is precisely what we do here.

In what follows we briefly describe the simulation methods, an extension of those used in [12], before going on to discuss the analysis of the results and our best estimates for the various exponents for the Ising, 4-state Potts and 10-state Potts models. We finish with some observations on the values we obtain.

2 Simulation and Measurements

We used the standard definition of the q -state Potts model partition function and energy in all the simulations,

$$Z_{\text{Potts}} = \sum_{\{\sigma_i\}} e^{-\beta E}; \quad E = - \sum_{\langle ij \rangle} \delta_{\sigma_i \sigma_j}; \quad \sigma_i = 1, \dots, q, \quad (5)$$

where $\beta = J/k_B T$ is the inverse temperature in natural units, δ is the Kronecker symbol, and $\langle ij \rangle$ denotes the nearest-neighbour bonds of random Φ^3 graphs (without tadpoles or self-energy bubbles) with N sites. In this study we considered the cases $q = 2$ and 4 (with $N = 500, 1\,000, 2\,000, 3\,000, 4\,000, 5\,000$, and 10 000) which in the pure model exhibit second-order phase transitions, and the case $q = 10$ (with $N = 250, 500, 1\,000, 2\,000, 3\,000, 5\,000$, and 10 000) which in the pure model undergoes a first-order phase transition.

The simulations were carried out using the Wolff single-cluster update algorithm [16]. For each lattice size we generated 64 independent graphs using the Tutte algorithm [17], and performed 500K equilibration sweeps followed by up to 10 million measurement sweeps in order to obtain 500K independent measurement sweeps for each lattice size. The runs were carried out at several β values near the transition point and time series of the energy E and the magnetisation² $M = (q \max\{n_i\} - N)/(q - 1)$ recorded for each graph. In what follows the per-site quantities are denoted by $e = E/N$ and $m = M/N$, the thermal averages on each individual graph by $\langle \dots \rangle$ and the quenched average over the different graphs by $[\dots]_{\text{av}}$.

From the time series of e and m it is straightforward to compute in the finite-size scaling (FSS) region various quantities at nearby values of β by standard reweighting [18] techniques. Some

¹Rather than average.

²Where $n_i \leq N$ denotes the number of spins of “orientation” $i = 1, \dots, q$ in one lattice configuration.

care must be taken with the reweighting range in the presence of quenched averaging, but we confirmed that direct measurements of both the susceptibility and specific heat from fluctuations and numerical derivatives were in accordance with the values deduced from reweighting in several representative cases. Comparisons for $q = 10$ and $N = 2000$ around the reweighting point of $\beta_0 = 2.22$ are shown in Figs. 1 and 2.

To estimate the statistical (thermal) errors for each of the 64 realizations, the time-series data was split into bins, which were jack-knifed [19] to decrease the bias in the analysis of reweighted data. The final values are averages over the 64 realizations which will be denoted by square brackets $[\dots]_{\text{av}}$, and the error bars are computed from the fluctuations among the realizations. Note that these errors contain both the average thermal error for a given realization and the theoretical variance for infinitely accurate thermal averages which is caused by the variation over the random graphs.

From the time series of the energy measurements we compute by reweighting the average energy, specific heat, and energetic fourth-order cumulant,

$$\begin{aligned} u(\beta) &= [\langle E \rangle]_{\text{av}}/N, \\ C(\beta) &= \beta^2 N [\langle e^2 \rangle - \langle e \rangle^2]_{\text{av}}, \\ V(\beta) &= [1 - \frac{\langle e^4 \rangle}{3\langle e^2 \rangle^2}]_{\text{av}}. \end{aligned} \tag{6}$$

Similarly, we derive from the magnetisation measurements the average magnetisation, susceptibility, and magnetic cumulants ³,

$$\begin{aligned} m(\beta) &= [\langle |m| \rangle]_{\text{av}}, \\ \chi(\beta) &= \beta N [\langle m^2 \rangle - \langle |m| \rangle^2]_{\text{av}}, \\ U_2(\beta) &= [1 - \frac{\langle m^2 \rangle}{3\langle |m| \rangle^2}]_{\text{av}}, \\ U_4(\beta) &= [1 - \frac{\langle m^4 \rangle}{3\langle m^2 \rangle^2}]_{\text{av}}. \end{aligned} \tag{7}$$

Further useful mixed quantities involving both the energy and magnetisation are defined by

$$\begin{aligned} \frac{d[\langle |m| \rangle]_{\text{av}}}{d\beta} &= [\langle |m| E \rangle - \langle |m| \rangle \langle E \rangle]_{\text{av}}, \\ \frac{d \ln[\langle |m| \rangle]_{\text{av}}}{d\beta} &= \left[\frac{\langle |m| E \rangle}{\langle |m| \rangle} - \langle E \rangle \right]_{\text{av}}, \\ \frac{d \ln[\langle m^2 \rangle]_{\text{av}}}{d\beta} &= \left[\frac{\langle m^2 E \rangle}{\langle m^2 \rangle} - \langle E \rangle \right]_{\text{av}}. \end{aligned} \tag{8}$$

The dynamical aspects of the simulations are encoded in the autocorrelation functions and the associated integrated autocorrelation times $\hat{\tau}$. It is customary [20] to convert the $\hat{\tau}$ thus obtained by multiplying with a factor $f = n_{\text{flip}} \langle |C| \rangle / N$ to a scale where, on the average, measurements are taken after every spin has been flipped once (similar to, e.g., Metropolis simulations). For quenched, random systems this procedure is not unique due to the necessary average over realizations, since one can take either $[\tau]_{\text{av}} \equiv [f \cdot \hat{\tau}]_{\text{av}}$ or $[f]_{\text{av}} \cdot [\hat{\tau}]_{\text{av}}$. The differences between the two averaging prescriptions turn out, however, to be extremely small in practice.

³See below for some subtleties in the ordering of averages in the cumulants.

One finds that the autocorrelation times for $q = 2$ stay roughly constant with increasing system size, being $[\tau_e]_{\text{av}} \sim 3 - 4$ for the energy and $[\tau_m]_{\text{av}} \sim 1.6 - 2.2$ for the magnetisation. For $q = 4$ scaling behaviour is visible with $[\tau_e]_{\text{av}} \sim 12 - 18$ and $[\tau_m]_{\text{av}} \sim 7 - 10$, giving a dynamical exponent $z/D \sim 0.064(10)$ for the energy. Power law scaling is much more pronounced for the $q = 10$ model with $[\tau_e]_{\text{av}} \sim 60 - 500$ and $[\tau_m]_{\text{av}} \sim 40 - 350$ and much larger dynamical exponents for both the energy and magnetisation, $z/D \sim O(1)$.

The self-averaging properties of the ensemble can be investigated by considering the probability density for the τ 's, $P(\tau)$, rather than the average values, $[\tau_{e,m}]_{\text{av}}$. One would expect the cumulative distribution $F(\tau) = \int_0^\tau P(\tau')d\tau'$ to tend to a step function for increasing system size in a self-averaging system. This is observed *not* to be the case for all the models simulated, giving clear evidence of non-self-averaging behaviour. These observations can be put on a more quantitative basis by looking at data collapse with the scaled variable $\Delta\tau/[\tau]_{\text{av}}$ [21], where $\Delta\tau$ is the standard deviation.

3 Data Analysis and Results

In the infinite-volume limit the various measured quantities exhibit singularities at the transition point. In finite systems the singularities are smeared out and scale in the critical region according to

$$\begin{aligned}
C &= C_{\text{reg}} + N^{\alpha/\nu D} f_C(x)[1 + \dots], \\
\chi &= N^{\gamma/\nu D} f_\chi(x)[1 + \dots], \\
[\langle |m| \rangle]_{\text{av}} &= N^{-\beta/\nu D} f_m(x)[1 + \dots], \\
\frac{d[\langle |m| \rangle]_{\text{av}}}{d\beta} &= N^{(1-\beta)/\nu D} f_{m'}(x)[1 + \dots], \\
\frac{d \ln[\langle |m|^p \rangle]_{\text{av}}}{d\beta} &= N^{1/\nu D} f_p(x)[1 + \dots], \\
\frac{dU_p}{d\beta} &= N^{1/\nu D} f_{U_{2p}}(x)[1 + \dots],
\end{aligned} \tag{9}$$

where C_{reg} is a regular background term, ν , α , β , and γ , are the usual critical exponents, and the $f_i(x)$ are various FSS functions with

$$x = (\beta - \beta_c)N^{1/\nu D} \tag{10}$$

being the scaling variable. $[1 + \dots]$ indicates correction terms which become unimportant for sufficiently large system sizes N . We have expressed the scaling relations in terms of the total number of vertices N rather than the linear size L since the fractal dimension D of the graphs is *a priori* unknown. Numerical simulations and various analytic approaches suggest that $D = 4$ [22] for the ensemble of graphs we are considering, but we shall not need this explicitly for our analysis here. By rearranging equ.(10) one finally obtains the standard scaling relation for the peak-locations (pseudo-critical points) $\beta_c(N)$ on finite graphs,

$$\beta_c(N) = \beta_c + aN^{-1/\nu D}, \tag{11}$$

with a being a constant.

One further issue of principle remains. In the presence of quenched disorder there are three equally plausible ways of defining the various cumulants. For instance, if we take the fourth order magnetic cumulant as an example we could define not only the form used above

$$U_4^{(1)} = \left[1 - \frac{\langle m^4 \rangle}{3 \langle m^2 \rangle^2} \right]_{\text{av}}, \quad (12)$$

but also the variants

$$\begin{aligned} U_4^{(2)} &= 1 - \frac{[\langle m^4 \rangle]_{\text{av}}}{3 [\langle m^2 \rangle^2]_{\text{av}}}, \\ U_4^{(3)} &= 1 - \frac{[\langle m^4 \rangle]_{\text{av}}}{3 [\langle m^2 \rangle^2]_{\text{av}}}, \end{aligned} \quad (13)$$

and the correct choice is not immediately clear. We can hedge our bets in the scaling analysis by including all three of the variants without prejudice in order to check their consistency. In simulations with poor statistics per realisation (such as typically in spin-glass studies) usually $U_4^{(3)}$ is taken since with that choice (systematic) bias effects are minimised. In our case, however, the statistics for each realisation is so large that there is no reason to favour one definition over the other on technical grounds.

Without further ado, we start the analysis by estimating the value of $1/\nu D$. With the wealth of available estimators we have various tactics available for the extraction of $1/\nu D$. One possibility would be to use the maxima of each of $dU_2/d\beta$, $dU_4/d\beta$ (all variants for both cumulants), $d \ln[\langle |m| \rangle]_{\text{av}}/d\beta$, and $d \ln[\langle m^2 \rangle]_{\text{av}}/d\beta$ as pseudo-critical points and then evaluate the scaling of each of these quantities at their own maxima to extract the exponent. Another would be to evaluate the scaling of each of these quantities at *all* of the available pseudo-critical points. A global estimate is then extracted by performing a direct or error weighted average. In both these cases we take a fairly conservative estimate for the errors by using the smallest contributing error bar ⁴.

We present the results from both approaches in Table 1. In obtaining these estimates we have dropped the smallest graph sizes in all cases and used $U^{(1)}$ for definiteness as our definition of the cumulants for the results presented in the table: $U^{(2)}$ and $U^{(3)}$ give values that are indistinguishable within the error bars. The results are quite stable to the deletion of the next smallest size, but the quality of the fits declines somewhat when this is done. In all of the listed fits the quality of fit Q was very good, the lowest being ≈ 0.3 , with most being as high as $0.8 - 0.9$. For comparison we have included the prediction of the quenched KPZ formula (equ.(2)), the standard KPZ exponents and the regular 2D lattice exponents in the lower box. Since the $q = 10$ model has a first-order transition on a regular 2D lattice there is no direct prediction in this case.

⁴The *largest* contributing error bar would certainly be too pessimistic; this choice probably errs on the side of caution too.

Table 1: *Fit results for the critical exponent $1/\nu D$.*

quantity	type	$q = 2$	$q = 4$	$q = 10$
$dU_2/d\beta$	at maximum	0.32(1)	0.42(2)	0.59(3)
	average	0.32(1)	0.45(2)	0.61(3)
	weighted av.	0.31(1)	0.44(2)	0.60(3)
$dU_4/d\beta$	at maximum	0.32(2)	0.39(2)	0.62(3)
	average	0.31(1)	0.40(2)	0.59(2)
	weighted av.	0.31(1)	0.40(2)	0.59(2)
$d \ln[\langle m \rangle]_{\text{av}}/d\beta$	at maximum	0.36(1)	0.42(1)	0.56(1)
	average	0.36(1)	0.43(1)	0.56(1)
	weighted av.	0.36(1)	0.43(1)	0.56(1)
$d \ln[\langle m^2 \rangle]_{\text{av}}/d\beta$	at maximum	0.36(1)	0.42(1)	0.56(1)
	average	0.36(1)	0.43(1)	0.57(1)
	weighted av.	0.36(1)	0.43(1)	0.57(1)
meta-average		0.34(1)	0.42(1)	0.58(1)
<i>Quenched</i>		0.3486 ...	0.589 ...	—
<i>KPZ</i>		0.3333 ...	0.5	—
<i>Regular</i>		0.5	0.75	—

Looking at the results in Table 1 it is clear that the estimates of $1/\nu D$ are not consistent with those for regular 2D lattices, giving a clear indication that the planar random graphs are different in this respect from Poissonian random lattices. The average of averages or “meta-average” for $q = 2$ is compatible with both the quenched and KPZ values at the level of accuracy we have achieved, but that for $q = 4$ matches none of the possible theoretical predictions. Remarkably, the estimated $q = 10$ values are a good fit to the quenched $q = 4$ predictions, as we have already noted in [12], and the numerous additional estimators here add extra weight to this observation. The difference between the theoretical quenched and KPZ values for $q = 4$ is sufficient for the $q = 10$ estimates *not* to be consistent with the theoretical $q = 4$ KPZ value.

It is also noteworthy that the $q = 10$ measurements (and also the $q = 4$ quenched theory predictions) violate a supposedly general bound derived by Chayes *et al.* [23] for quenched systems, $\nu D > 2$, since $\nu D \sim 1.72(3)$ from the $q = 10$ measurements. Hyperscaling, $\alpha/\nu D = 2/\nu D - 1$, implies that $\alpha/\nu D$ should be negative if the bound holds, but we find below that direct fits to the specific heat for $q = 10$ also give a positive value (0.21(1)) that is compatible with that deduced from hyperscaling (0.16(1)). The measured values of νD for $q = 2$ and $q = 4$, on the other hand, *are* consistent with the bound. Whether the failure of the $q = 10$ model to observe the bound is a consequence of the technical details of the averaging procedure as suggested in [24] or a result of long range correlations in the disorder (which is due to the curvature correlations for the Liouville action in the original 2D gravity theory used to generate the graphs) is unclear.

We now use our best estimates of $1/\nu D$ to extract the critical coupling β_c by performing a linear two-parameter fit, equ.(11), using the maxima of C and χ along with derivatives of the three variants of U_2 and U_4 and derivatives and logarithmic derivatives of the magnetization as estimators of the pseudocritical points. This gives the eleven estimators which are shown in Table 2. A global estimate is again extracted by performing both a straightforward average and

an error weighted average. It is noteworthy that the estimated critical couplings are compatible with those found in simulations of the models coupled to 2D quantum gravity ⁵, i.e., with *annealed* rather than quenched connectivity disorder. This was already remarked on in [12, 13] where non-linear three parameter fits were employed.

Table 2: *Fit results for the pseudocritical couplings β_c .*

at β_{\max} of	$q = 2$	$q = 4$	$q = 10$
C	1.539(5)	1.836(1)	2.244(1)
χ	1.562(6)	1.834(2)	2.246(1)
$dU_2^{(1)}/d\beta$	1.551(5)	1.831(1)	2.244(1)
$dU_2^{(2)}/d\beta$	1.550(5)	1.834(1)	2.242(1)
$dU_2^{(3)}/d\beta$	1.550(5)	1.831(2)	2.243(1)
$dU_4^{(1)}/d\beta$	1.558(7)	1.832(2)	2.244(1)
$dU_4^{(2)}/d\beta$	1.569(4)	1.841(2)	2.240(2)
$dU_4^{(3)}/d\beta$	1.562(5)	1.834(2)	2.242(1)
$d\langle m \rangle/d\beta$	1.561(3)	1.834(1)	2.245(1)
$d\log\langle m \rangle/d\beta$	1.562(5)	1.837(2)	2.243(1)
$d\log\langle m^2 \rangle/d\beta$	1.570(5)	1.838(1)	2.243(1)
average	1.558(3)	1.835(1)	2.244(1)
weighted av.	1.558(3)	1.835(1)	2.244(1)

The crossing points of the various definitions of the fourth-order cumulant in eqs. (12) and (13) provide further estimates of β_c . The error bars from these measurements are much larger than those in Table 2 due to the spread of crossings for different system sizes, but the estimates from $U_4^{(1)}$, $U_4^{(2)}$, and $U_4^{(3)}$ are all consistent, giving $\beta_c = 1.58(2)$ for $q = 2$, $\beta_c = 1.85(2)$ for $q = 4$, and $\beta_c = 2.244(4)$ for $q = 10$. The rather wide spread in the estimated β_c is reflected by a similar spread in the values of U_4 at β_c , usually denoted by U^* . The variant $U_4^{(2)}$ appears to be the best behaved for all q giving $U^* \approx 0.55(3)$.

Moving on to $\alpha/\nu D$, the Fisher hyperscaling relation in the form

$$\frac{\alpha}{\nu D} = \frac{2}{\nu D} - 1 \quad (14)$$

gives $\alpha/\nu D = -0.32(1)$, $-0.16(1)$, and $0.16(1)$ for $q = 2, 4$, and 10 , respectively, from the $1/\nu D$ values in Table 1, whereas the quenched predictions are $\alpha/\nu D = -0.303\dots$ and $0.177\dots$ for $q = 2$ and 4 . Direct non-linear fits to $\alpha/\nu D$ using the scaling form $C = C_{reg} + C_1 N^{\alpha/\nu D}$ for the maxima of the specific heat are unstable for $q = 2, 4$ but give $\alpha/\nu D = 0.22(7)$ for $q = 10$. The constant in this fit is consistent with zero, so we carried out a log-log fit at all of the pseudo-critical points as shown in Table 3, giving a final average of $\alpha/\nu D = 0.21(1)$ for $q = 10$. Two representative series of points for the specific heat evaluated at its own maximum and the maximum of the susceptibility on the different graph sizes are shown in Fig. 3. This independent measurement of $\alpha/\nu D$ when $q = 10$ is thus still in reasonable agreement with the theoretical quenched exponent values for $q = 4$.

⁵On corresponding ensembles of graphs without tadpoles and self-energy bubbles.

Table 3: *Fit results for the critical exponent $\alpha/\nu D$ for $q = 10$.*

at β_{\max} of	$q = 10$
C	0.21(1)
χ	0.21(2)
$dU_2^{(1)}/d\beta$	0.22(1)
$dU_2^{(2)}/d\beta$	0.21(1)
$dU_2^{(3)}/d\beta$	0.22(1)
$dU_4^{(1)}/d\beta$	0.21(1)
$dU_4^{(2)}/d\beta$	0.18(2)
$dU_4^{(3)}/d\beta$	0.21(1)
$d\langle m \rangle/d\beta$	0.21(1)
$d\log\langle m \rangle/d\beta$	0.21(1)
$d\log\langle m^2 \rangle/d\beta$	0.22(1)
average	0.21(1)
weighted av.	0.21(1)
$q = 4$ <i>Quenched</i>	0.177 ...
$q = 4$ <i>KPZ</i>	0
$q = 4$ <i>Regular</i>	0.5

In Tables 4, 5, and 6 we list the measured values of the magnetic exponents $\gamma/\nu D$, $\beta/\nu D$ and $(1 - \beta)/\nu D$ for $q = 2, 4$, and 10. We have adopted a similar approach to that used in the estimation of $1/\nu D$. Data from all but the smallest graph size was included in the fits, and the stability of the fits checked against the deletion of the next smallest sizes, proving in all the listed cases to be reasonable. The appropriate scaling relations in equ. (9) are evaluated at all the pseudo-critical points reported in the tables and a final averaged value and error weighted average calculated. For the blank entries in the tables no stable fit proved possible. In the tables the number of terms used in the averages for each exponent are listed in the average row, and various theoretical predictions for the exponents are listed for comparison. Since it is already clear that the $q = 10$ measurements bear a considerable similarity to the quenched $q = 4$ predictions we have repeated the $q = 4$ theoretical values in the $q = 10$ table. The exponent ratio $\gamma/\nu D$ is evaluated from the scaling of the susceptibility χ , $\beta/\nu D$ from the scaling of the derivative of the magnetisation and $(1 - \beta)/\nu D$ from the scaling of the logarithmic derivative.

The scaling relation

$$\frac{\gamma}{\nu D} = 1 - 2\frac{\beta}{\nu D} \quad (15)$$

relates the two exponents in these tables. The directly measured values are all in reasonable agreement with those derived by using either exponent as input in this scaling relation. There is an accidental equality between the theoretical quenched values of $\gamma/\nu D$ (and hence via equ.(15) of $\beta/\nu D$) for the Ising and 4-state Potts models which is not, however, reflected in the estimates. There is a steady decrease in $\gamma/\nu D$ and corresponding increase in $\beta/\nu D$ as q is increased, so the $q = 4$ and $q = 10$ measurements are clearly different from those for $q = 2$. There is still a striking agreement between the quenched $q = 4$ predictions and the measurements at $q = 10$. It

is also clear that the $q = 4$ measurements are in definite disagreement with the quenched $q = 4$ predictions.

In Fig. 4 we plot the data points and fits for the susceptibility in the Ising model. The individual points for χ evaluated at its own maximum, the maximum of the specific heat, the maxima of the derivatives of the second and fourth order cumulants and the maximum of the derivative of the magnetisation are shown explicitly ⁶. The fits from the different series are all in good agreement, as indicated by the tables. We also plot χ evaluated at its own maximum for $q = 2, 4,$ and 10 in Fig. 5 in order to show the general trend in the exponent.

4 Conclusions

The qualitative conclusions of our extensive analyses are quite clear: the quenched bond disorder of the Φ^3 graphs *does* alter the exponents of models which already possess a continuous transition on a regular lattice, as well as softening the first-order transition of the $q = 10$ model to a continuous transition. A quenched ensemble of Φ^3 graphs with connectivity disorder thus shares many of the features of a system with quenched bond disorder. As noted in the introduction, other ensembles with quenched connectivity disorder such as Poissonian random lattices do not – being more akin to regular lattices.

At a quantitative level, however, the current batch of simulations pose rather more questions than they answer: the working hypothesis of the veracity of the quenched exponents is at best only weakly supported by the results. For the Ising ($q = 2$) model, the estimated value of $1/\nu D$, $0.34(1)$, is consistent with both the quenched and KPZ predictions. Although the estimates for the magnetic exponents $[\gamma/\nu D, \beta/\nu D, (1 - \beta)/\nu D] \sim [0.79(1), 0.11(1), 0.26(1)]$ are closer to the quenched $[0.7094, 0.1452, 0.2033]$ than the Onsager $[0.875, 0.0625, 0.4375]$ or KPZ $[0.666\dots, 0.166\dots, 0.166\dots]$ values, any agreement is less than convincing. In mitigation, it is fair to point out that we have struggled in the past to obtain good estimates of the magnetic KPZ exponents on dynamical Φ^3 graphs without tadpoles and self-energy bubbles [25], which is the class of graph we have used in the simulations here. This is probably due to large corrections to scaling, since including degenerate graphs (self-energy bubbles and tadpoles) appears to give a faster approach to the continuum limit [26].

Taken *en masse* the estimated exponents of the $q = 4$ model, $[1/\nu D, \gamma/\nu D, \beta/\nu D, (1 - \beta)/\nu D] \sim [0.42(1), 0.75(1), 0.12(1), 0.34(1)]$ fit neither the quenched $[0.589\dots, 0.7094\dots, 0.1452\dots, 0.4433\dots]$, KPZ $[0.5, 0.5, 0.25, 0.25]$ nor regular lattice $[0.75, 0.875, 0.0625, 0.6875]$ predictions, although one could argue that $\gamma/\nu D \sim 0.75(1)$ on its own is actually closer to the quenched prediction than the $q = 2$ model. It is possible that $q = 4$, which is subject to logarithmic corrections in both the regular lattice and KPZ cases, may require similar treatment in the quenched case but without more input on the form of these corrections fitting would be a futile exercise.

The $q = 10$ model, on the other hand, provides us with a set of estimated exponents $[1/\nu D, \gamma/\nu D, \beta/\nu D, (1 - \beta)/\nu D] \sim [0.58(1), 0.71(1), 0.12(1), 0.43(2)]$ which match the predicted quenched $q = 4$ exponents $[0.589\dots, 0.7094\dots, 0.1452\dots, 0.4433\dots]$ extremely well. These estimated $q = 10$ exponents (and theoretical $q = 4$ values) hence violate the bound $\nu D > 2$ of [23], which merits an explanation in its own right.

⁶We have shown only the $U_{2,4}^{(1)}$ cumulant results to avoid cluttering the graph, the alternative definitions give effectively identical results. χ evaluated at the maxima of the derivatives of the log of the magnetisation and the modulus squared of the magnetisation has also been dropped for clarity. The graphs for $q = 4$ and $q = 10$ show similar features and are not reproduced here.

It is difficult to quibble with the thermal statistics from the very long time series in the current batch of simulations, but one might find fault with the relatively modest number of replicas used in the disorder averaging. The replica to replica variation of the measured quantities does not, however, appear to have significantly skewed the measured values and error estimates. Looked at without theoretical prejudice the measured exponents suggest a slow variation with q that is akin to that observed in the quenched bond disorder simulations of [4], rather than values which stick at $q = 4$ and change no further with increasing q . It is thus possible that the agreement of the measured $q = 10$ exponents with the predicted $q = 4$ values is accidental. A simple way to settle this issue would be to simulate other values of q to investigate the variation, if any, of the exponents, particularly for $q > 4$.

There is a second parameter that one can vary in such simulations, namely the central charge used in generating the graphs of the quenched ensemble. Since the partition function Z_N obtained on integrating out d scalar fields on Φ^3 graphs with N vertices is

$$Z_N = \sum_{G \in \mathcal{G}(A)} (\det C_G)^{-d/2}, \quad (16)$$

where $\mathcal{G}(A)$ is the class of graph being summed over and C_G is the adjacency matrix of the graph G ,

$$C_G = \begin{cases} q_i & \text{if } i = j, \\ -n_{ij} & \text{if } i \text{ and } j \text{ are adjacent,} \\ 0 & \text{otherwise,} \end{cases} \quad (17)$$

one can use equ.(16) to generate an ensemble of graphs to which one can associate a central charge d .

Quenched simulations may then be carried out on this ensemble rather than the $d = c = 0$ graphs used here. The appropriate d can be substituted into the *KPZ* formula to obtain predictions for the exponents in this case. This brings one to another puzzle: in [27] very good agreement was found between the predicted exponents for the Ising model on a quenched ensemble of graphs with $d = -5$ and measurements. In this light, it is surprising that the agreement here for the Ising model on much larger $d = 0$ graphs with better statistics is poorer. One could speculate that the scaling behaviour of the models improved as they became more “classical”, i.e. as the effects of gravity were switched off ($d \rightarrow -\infty$).

Various other aspects of the behaviour of spin models on quenched random gravity graphs that have only been touched on here merit further investigation. The clear evidence of non-self-averaging behaviour for all q and the autocorrelation scaling techniques used to quantify it are described in more detail in a companion paper [21]. Similarly, the multifractal scaling of spin correlation functions can also be investigated. Finally, as we have already noted, further simulations for other q (and also d) values would help to determine whether the quenched exponents were correctly describing the behaviour of the models and cast further light on the remarkable (accidental?) agreement between $q = 10$ measurements and the predicted $q = 4$ exponents.

In summary, spin models on Φ^3 random graphs offer a useful framework for the exploration of quenched disorder and may even offer some advantages over bond disordered models given the availability of various exact, rather than perturbative, predictions for exponents. The results described here suggest numerous avenues for future work.

Acknowledgements

DJ was partially supported by a Royal Society of Edinburgh/SOEID Support Research Fellowship. WJ acknowledges partial support by the German-Israel-Foundation (GIF) under contract No. I-0438-145.07/95. The collaborative work of DJ and WJ was funded by ARC grant 313-ARC-XII-98/41. The numerical simulations were performed on a T3D parallel computer of Zuse-Zentrum für Informationswissenschaften Berlin (ZIB) under grant No. bvpf01.

References

- [1] For a review, see J. Cardy, “Quenched Randomness at First-Order Transitions”, invited talk at STATPHYS20, Paris, July 1998, published in: *Physica* **A263**, 215 (1999) [**cond-mat/9806355**].
- [2] A. B. Harris, *J. Phys. C* **7**, 1671 (1974);
Y. Imry and M. Wortis, *Phys. Rev. B* **19**, 3581 (1979);
M. Aizenman and J. Wehr, *Phys. Rev. Lett.* **62**, 2503 (1989);
K. Hui and A. N. Berker, *Phys. Rev. Lett.* **62**, 2507 (1989); *Phys. Rev. Lett.* **63**, 2433 (1989) (erratum).
- [3] S. Chen, A. M. Ferrenberg, and D. P. Landau, *Phys. Rev.* **E52**, 1377 (1995);
M. Kardar, A. L. Stella, G. Sartoni, and B. Derrida, *Phys. Rev.* **E52**, R1269 (1995);
S. Wiseman and E. Domany, *Phys. Rev.* **E51**, 3074 (1995); *ibid.* **E52**, 3469 (1995).
- [4] J. Cardy and J. L. Jacobsen, *Phys. Rev. Lett.* **79**, 4063 (1997);
J. L. Jacobsen and J. L. Cardy, *Nucl. Phys. B* **515**, 701 (1998);
C. Chatelain and B. Berche, *Phys. Rev. Lett.* **80**, 1670 (1998).
- [5] A. W. W. Ludwig and J. L. Cardy, *Nucl. Phys. B* **285** [FS19], 687 (1987);
A. W. W. Ludwig, *Nucl. Phys. B* **285**, 97 (1987);
V. Dotsenko and V. Dotsenko, *Sov. Phys. JETP Lett.* **33**, 37 (1981); *Adv. Phys.* **32**, 129 (1983);
V. Dotsenko, M. Picco, and P. Pujol, *Phys. Lett. B* **347**, 113 (1995); *Nucl. Phys. B* **455**, 701 (1995).
- [6] V.B. Andreichenko, V.I.S. Dotsenko, W. Selke, and J.-S. Wang, *Nucl. Phys.* **B344**, 531 (1990);
J.-S. Wang, W. Selke, V.I.S. Dotsenko, and V.B. Andreichenko, *Europhys. Lett.* **11**, 301 (1990);
J.-S. Wang, W. Selke, V.I.S. Dotsenko, and V.B. Andreichenko, *Physica* **A164**, 221 (1990);
A.L. Talapov and L.N. Shchur, *J. Phys. Condens. Matter* **6**, 8295 (1994); F.D.A. Aarão Reis, S.L.A. de Queiroz, and R.R. dos Santos, *Phys. Rev.* **B56**, 6013 (1997).
- [7] A. Roder, J. Adler, and W. Janke, *Phys. Rev. Lett.* **80**, 4697 (1998); *Physica* **A265**, 28 (1999).
- [8] J. Cardy, *J. Phys.* **A32**, L177 (1999).
- [9] T. Olson and A.P. Young, preprint cond-mat/9903068 (1999).

- [10] W. Janke, M. Katoot, and R. Villanova, Phys. Lett. **B315**, 412 (1993); Nucl. Phys. **B** (Proc. Suppl.) **34**, 698 (1994); Phys. Rev. **B49**, 9644 (1994);
W. Janke and R. Villanova, Phys. Lett. **A209**, 179 (1995); Nucl. Phys. **B** (Proc. Suppl.) **47**, 641 (1996).
- [11] W. Janke and R. Villanova, in preparation.
- [12] C. Baillie, W. Janke, and D. Johnston, Phys. Lett. **B388**, 14 (1996);
Nucl. Phys. **B** (Proc. Suppl.) **53**, 732 (1997).
- [13] C.F. Baillie, K.A. Hawick, and D.A. Johnston, Phys. Lett. **B328**, 284 (1994).
- [14] D. Johnston, Phys. Lett. **B277**, 405 (1992).
- [15] V.G. Knizhnik, A.M. Polyakov, and A.B. Zamolodchikov, Mod. Phys. Lett. **A3**, 819 (1988);
F. David, Mod. Phys. Lett. **A3**, 1651 (1988);
J. Distler and H. Kawai, Nucl. Phys. **B321**, 509 (1989).
- [16] U. Wolff, Phys. Rev. Lett. **62**, 361 (1989); Nucl. Phys. **B334**, 581 (1990).
- [17] M.E. Agishtein and A.A. Migdal, Nucl. Phys. **B350**, 690 (1991);
W. Tutte, Can. J. of Math. **14**, 21 (1962); *ibid* **15**, 249 (1963).
- [18] A.M. Ferrenberg and R.H. Swendsen, Phys. Rev. Lett. **61**, 2635 (1988); and *Erratum*, *ibid.* **63**, 1658 (1989).
- [19] R.G. Miller, Biometrika **61**, 1 (1974); B. Efron, *The Jackknife, the Bootstrap and other Resampling Plans* (SIAM, Philadelphia, PA, 1982).
- [20] U. Wolff, Phys. Rev. Lett. **62**, 361 (1989); Nucl. Phys. **B334**, 581 (1990).
- [21] W. Janke and D.A. Johnston, in preparation.
- [22] J. Ambjørn, K.N. Anagnostopoulos, T. Ichihara, L. Jensen, and Y. Watabiki, JHEP 9811 (1998) 022;
J. Ambjørn, K. N. Anagnostopoulos, and G. Thorleifsson, Nucl. Phys. **B** (Proc. Suppl.) **63**, 742 (1998);
J. Ambjørn and K.N. Anagnostopoulos, Nucl. Phys. **B497**, 445 (1997);
M. Bowick, V. John, and G. Thorleifsson, Phys. Lett. **B403**, 197 (1997).
- [23] J. T. Chayes, L. Chayes, D. S. Fisher, and T. Spencer, Phys. Rev. Lett. **57**, 2999 (1986);
J. T. Chayes, L. Chayes, D. S. Fisher, and T. Spencer, Commun. Math. Phys. **120**, 501 (1989).
- [24] F. Pázmándi, R. T. Scalettar, and G. T. Zimányi, Phys. Rev. Lett. **79**, 5130 (1997).
- [25] C.F. Baillie and D.A. Johnston, Mod. Phys. Lett. **A7**, 1519 (1992); Phys. Lett. **B286**, 44 (1992).
- [26] J. Ambjørn, K. N. Anagnostopoulos, U. Magnea, and G. Thorleifsson, Phys. Lett. **B388**, 713 (1996).
- [27] K. Anagnostopoulos, P. Bialas, and G. Thorleifsson, “The Ising Model on a Quenched Ensemble of $c = -5$ Gravity Graphs”, preprint cond-mat/9804137 (1998).

Table 4: $q=2$ Potts (Ising) fit results for the critical exponents $\gamma/\nu D$, $\beta/\nu D$, and $(1 - \beta)/\nu D$.

at β_{\max} of	$\gamma/\nu D$	Q	$\beta/\nu D$	Q	$(1 - \beta)/\nu D$	Q
C	0.75(1)	0.14	0.14(2)	0.24	0.23(2)	0.40
χ	0.79(1)	0.13	0.08(1)	0.21	0.26(1)	0.78
$dU_4^{(1)}/d\beta$	0.79(2)	0.66	0.12(1)	0.42	0.26(2)	0.33
$dU_4^{(2)}/d\beta$	–	–	–	–	–	–
$dU_4^{(3)}/d\beta$	0.80(2)	0.46	0.10(1)	0.14	0.28(1)	0.13
$dU_2^{(1)}/d\beta$	0.77(1)	0.75	0.12(1)	0.82	0.25(1)	0.76
$dU_2^{(2)}/d\beta$	0.77(1)	0.73	0.12(1)	0.64	0.25(1)	0.63
$dU_2^{(3)}/d\beta$	0.77(1)	0.78	0.12(1)	0.84	0.25(1)	0.62
$d[\langle m \rangle]_{\text{av}}/d\beta$	–	–	0.09(1)	0.38	0.26(1)	0.80
$d\ln[\langle m \rangle]_{\text{av}}/d\beta$	0.80(1)	0.55	0.10(1)	0.36	0.28(1)	0.37
$d\ln[\langle m^2 \rangle]_{\text{av}}/d\beta$	0.83(2)	0.15	–	–	0.30(1)	0.32
average (9,9,10)	0.79(1)		0.11(1)		0.26(1)	
weighted av.	0.78(1)		0.10(1)		0.26(1)	
<i>Quenched</i>	0.7094 ...		0.1452 ...		0.2033 ...	
<i>KPZ</i>	0.6666 ...		0.1666 ...		0.1666 ...	
<i>Regular</i>	0.875		0.0625		0.4375	

Table 5: $q=4$ Potts fit results for the critical exponents $\gamma/\nu D$, $\beta/\nu D$, and $(1 - \beta)/\nu D$.

at β_{\max} of	$\gamma/\nu D$	Q	$\beta/\nu D$	Q	$(1 - \beta)/\nu D$	Q
C	–	–	–	–	–	–
χ	0.75(1)	0.13	–	–	0.34(2)	0.61
$dU_4^{(1)}/d\beta$	–	–	–	–	0.33(1)	0.37
$dU_4^{(2)}/d\beta$	–	–	–	–	–	–
$dU_4^{(3)}/d\beta$	–	–	–	–	–	–
$dU_2^{(1)}/d\beta$	0.75(1)	0.82	0.12(1)	0.50	0.33(1)	0.70
$dU_2^{(2)}/d\beta$	0.77(1)	0.42	–	–	0.34(1)	0.41
$dU_2^{(3)}/d\beta$	0.75(1)	0.80	0.13(1)	0.26	0.33(1)	0.66
$d[\langle m \rangle]_{\text{av}}/d\beta$	0.75(1)	0.44	0.10(1)	0.99	0.34(1)	0.73
$d\ln[\langle m \rangle]_{\text{av}}/d\beta$	–	–	–	–	–	–
$d\ln[\langle m^2 \rangle]_{\text{av}}/d\beta$	–	–	–	–	–	–
average (5,3,6)	0.75(1)		0.12(1)		0.34(1)	
weighted av.	0.75(1)		0.11(1)		0.34(1)	
<i>Quenched</i>	0.7094 ...		0.1452 ...		0.4433 ...	
<i>KPZ</i>	0.5		0.25		0.25	
<i>Regular</i>	0.875		0.0625		0.6875	

Table 6: $q=10$ Potts fit results for the critical exponents $\gamma/\nu D$, $\beta/\nu D$, and $(1 - \beta)/\nu D$.

at β_{\max} of	$\gamma/\nu D$	Q	$\beta/\nu D$	Q	$(1 - \beta)/\nu D$	Q
C	0.71(2)	0.13	–	–	–	–
χ	0.72(1)	0.31	0.10(1)	0.39	0.43(2)	0.10
$dU_4^{(1)}/d\beta$	0.73(2)	0.72	0.11(1)	0.23	0.43(2)	0.53
$dU_4^{(2)}/d\beta$	–	–	–	–	–	–
$dU_4^{(3)}/d\beta$	0.69(2)	0.30	–	–	0.41(2)	0.22
$dU_2^{(1)}/d\beta$	0.72(2)	0.61	0.12(1)	0.32	0.43(2)	0.19
$dU_2^{(2)}/d\beta$	–	–	–	–	0.42(2)	0.16
$dU_2^{(3)}/d\beta$	0.71(2)	0.37	0.14(1)	0.29	0.43(2)	0.12
$d[\langle m \rangle]_{\text{av}}/d\beta$	0.72(2)	0.25	0.11(1)	0.10	0.43(2)	0.11
$d\ln[\langle m \rangle]_{\text{av}}/d\beta$	0.71(2)	0.10	–	–	0.43(2)	0.10
$d\ln[\langle m^2 \rangle]_{\text{av}}/d\beta$	–	–	–	–	0.43(2)	0.11
average (8,5,9)	0.71(1)		0.12(1)		0.43(2)	
weighted av.	0.71(1)		0.12(1)		0.43(2)	
$q = 4$ <i>Quenched</i>	0.7094 ...		0.1452 ...		0.4433 ...	
$q = 4$ <i>KPZ</i>	0.5		0.25		0.25	
$q = 4$ <i>Regular</i>	0.875		0.0625		0.6875	

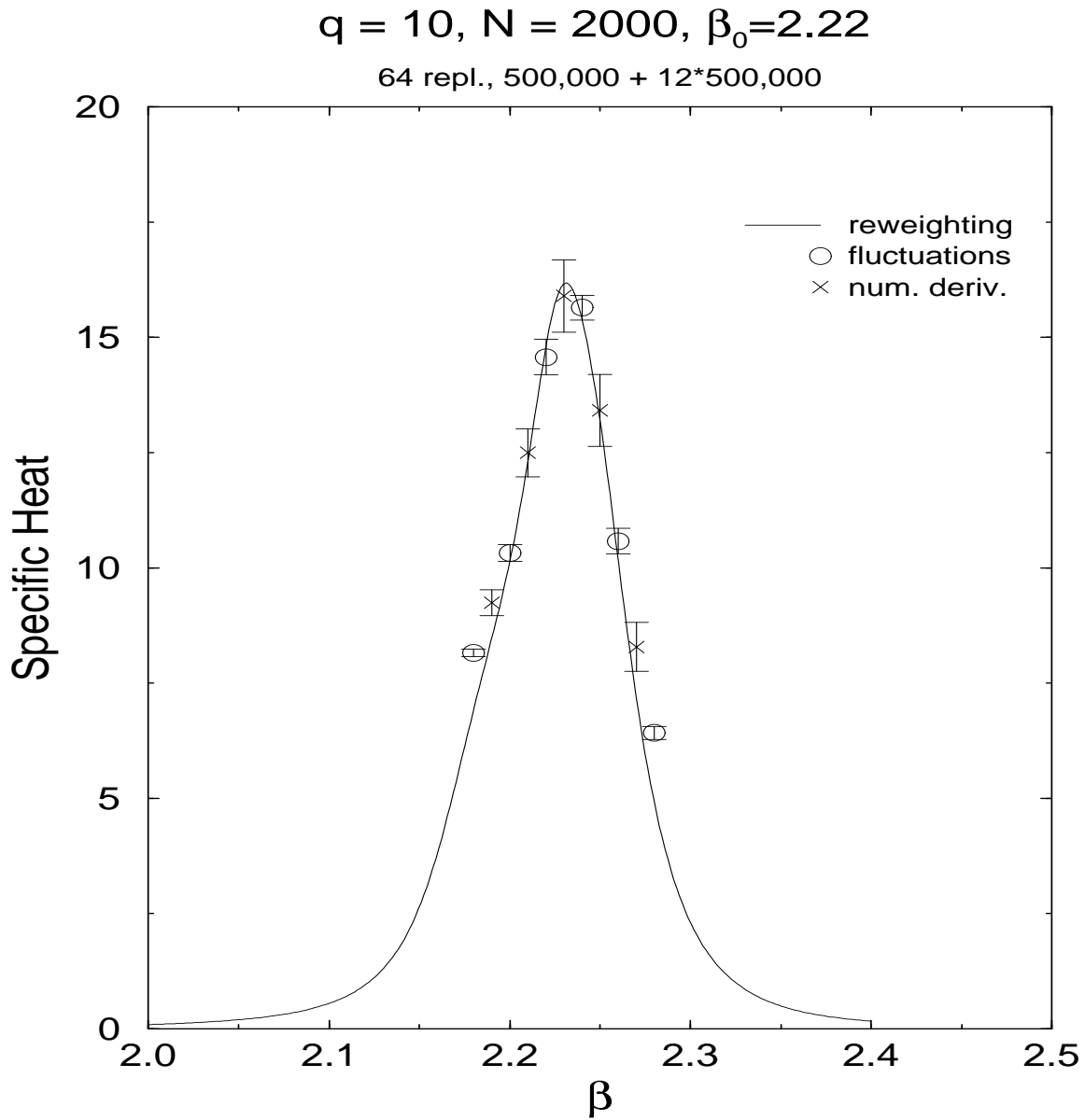


Figure 1: The specific heat calculated from reweighting about $\beta_0 = 2.22$, fluctuations and numerical differentiation of the energy for $q = 10$ and $N = 2000$ (which is typical).

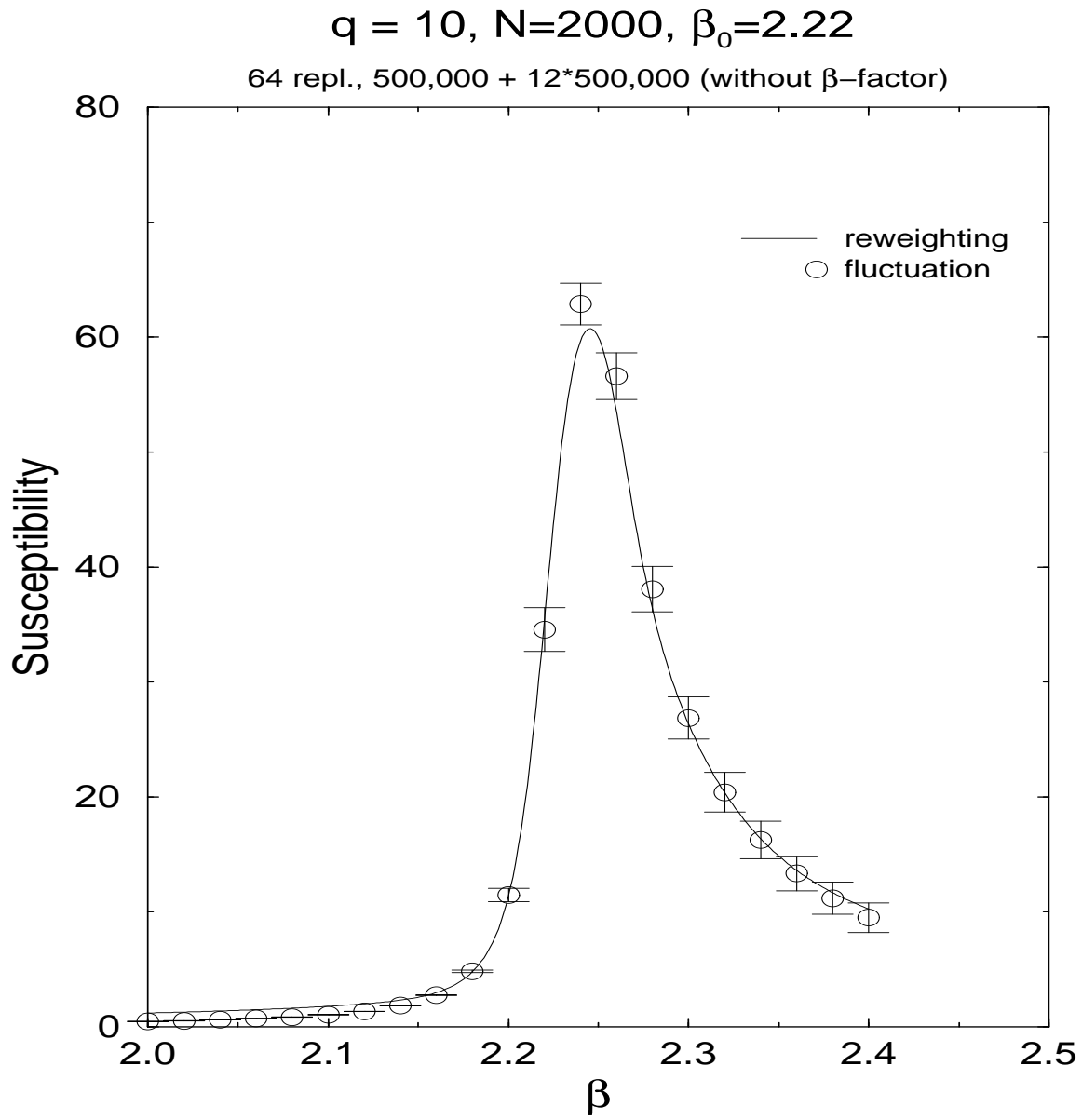


Figure 2: The susceptibility calculated from reweighting about $\beta_0 = 2.22$ and from fluctuations for $q = 10$ and $N = 2000$.

Specific Heat vs N for q=10

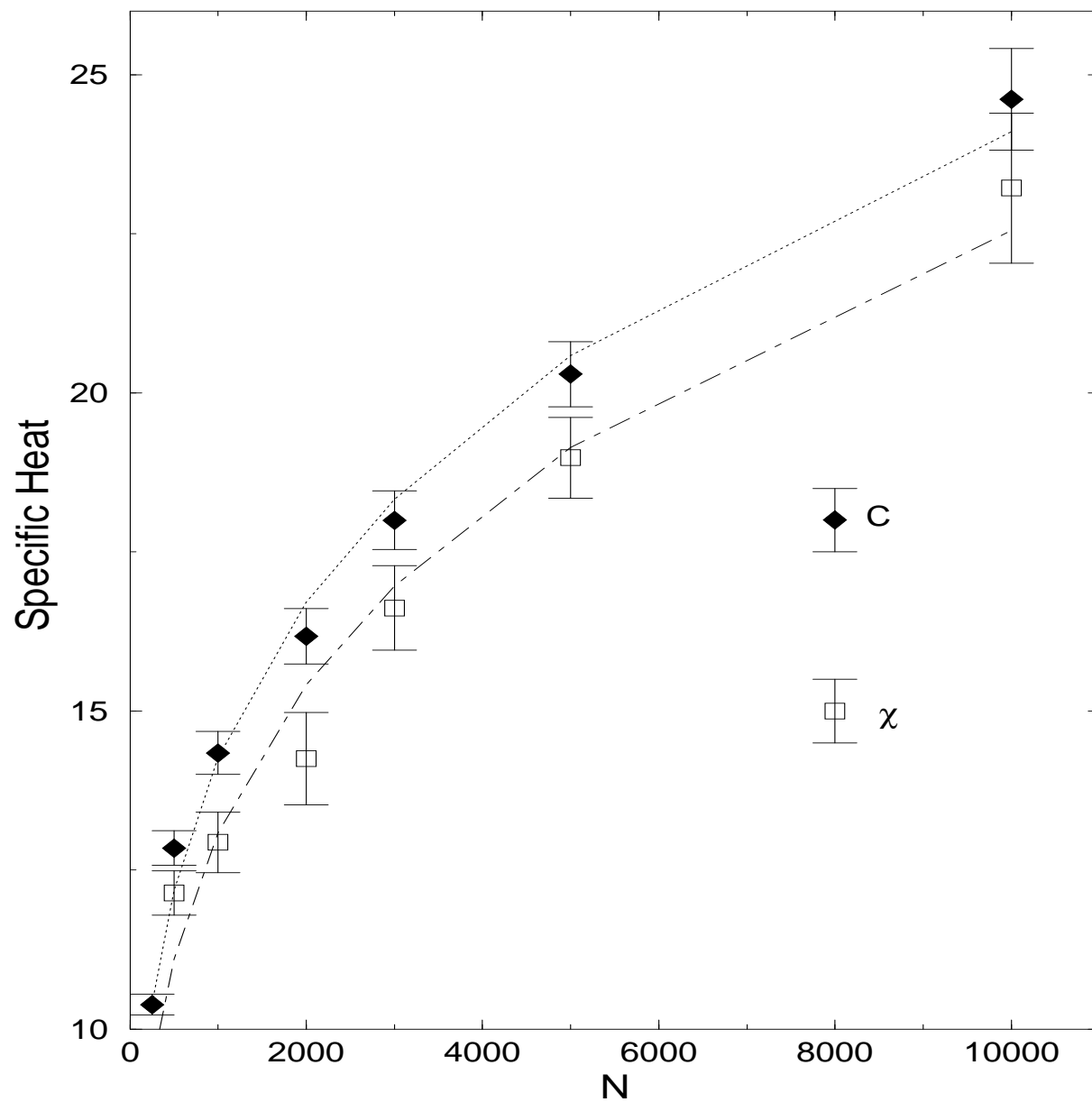


Figure 3: Two representative fits (from the eleven used) for the scaling of the specific heat evaluated at its own maximum and at the maximum of the susceptibility χ .

Susceptibility vs N for q=2

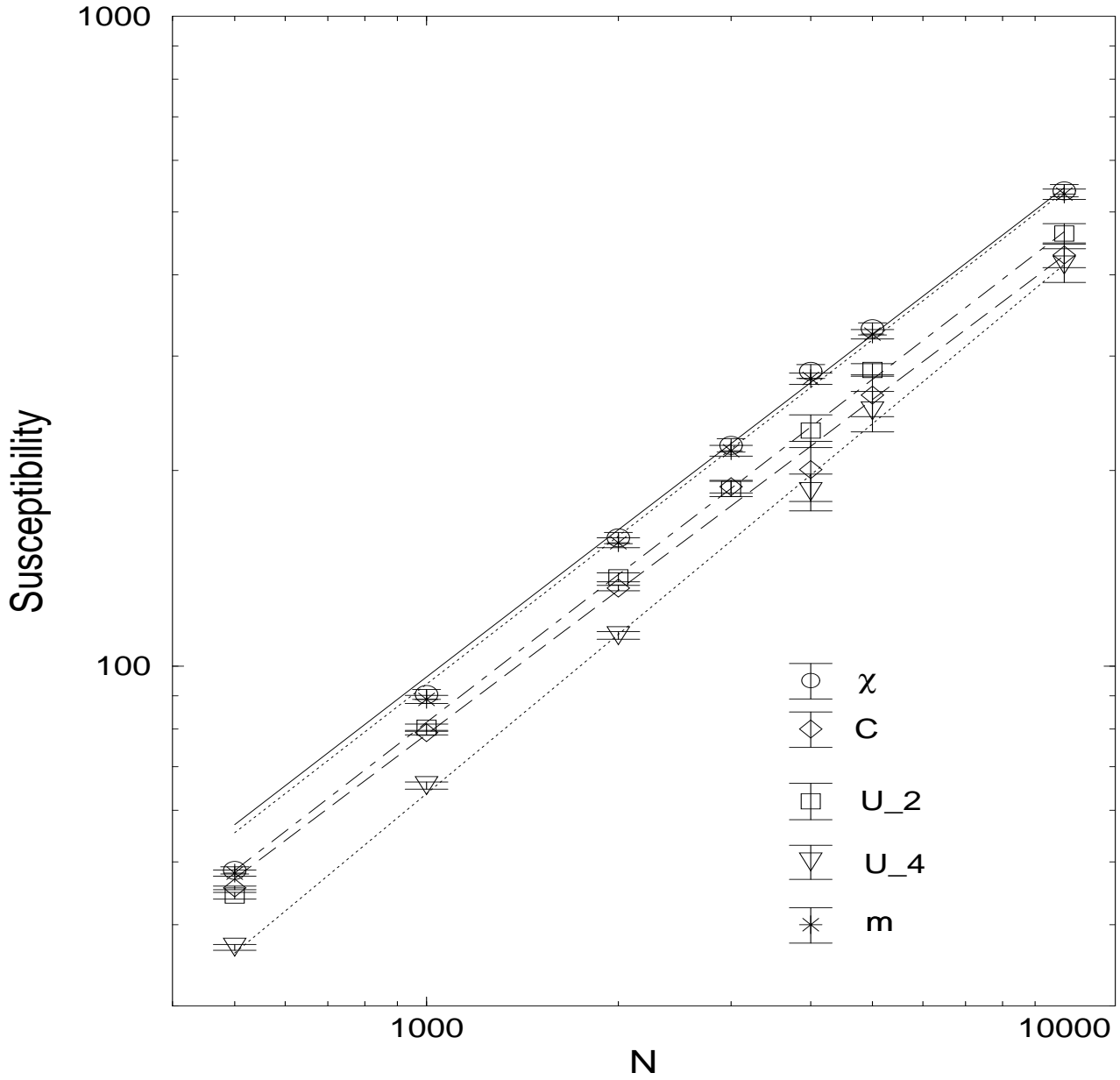


Figure 4: Fits to χ when $q = 2$ to obtain $\gamma/\nu D$ at the maxima of χ , C , $dU_2^{(1)}/d\beta$, $dU_4^{(1)}/d\beta$ and $dm/d\beta$ are shown on a log-log scale.

Susceptibility vs N for $q=2,4,10$

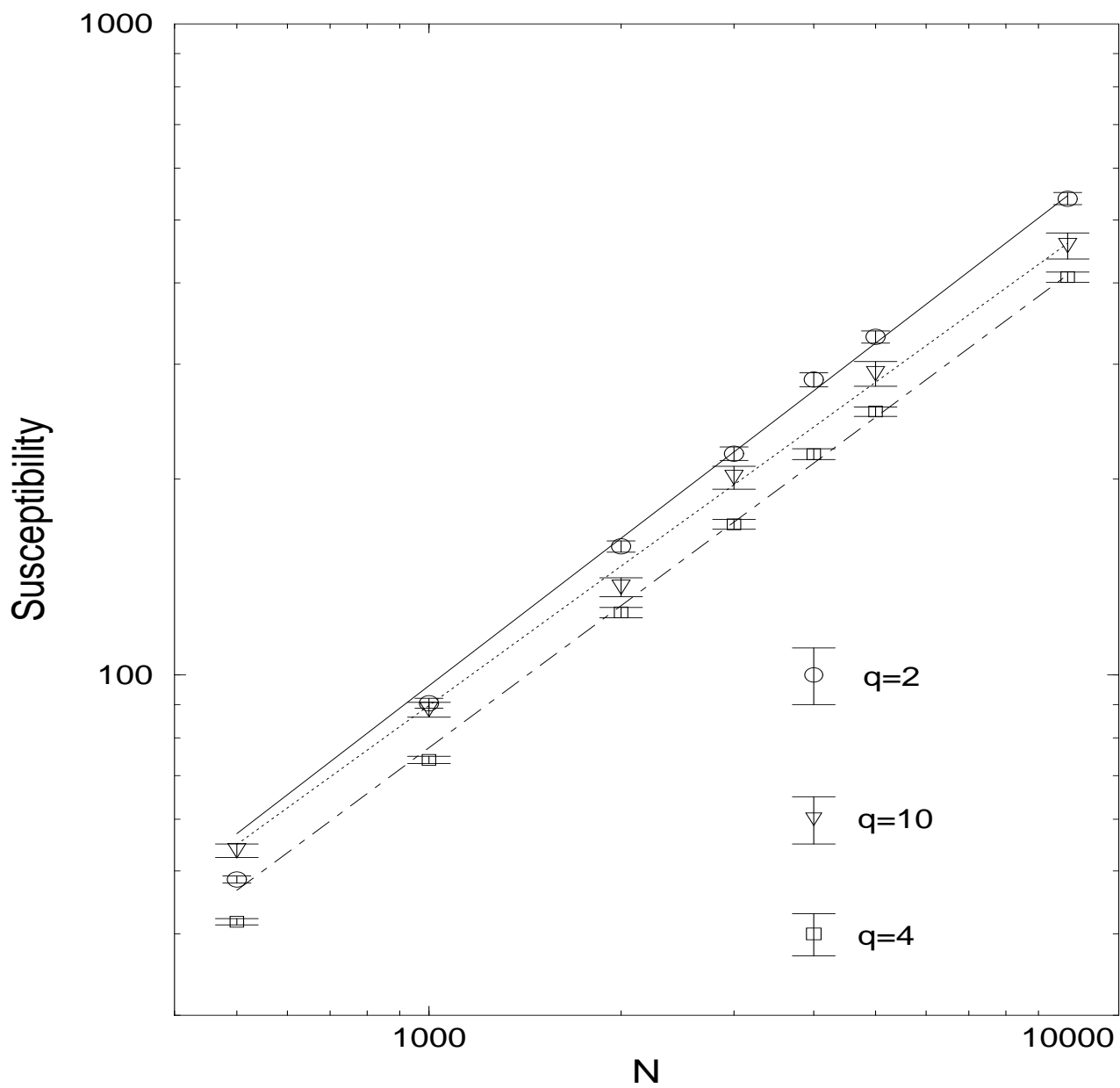


Figure 5: Fits to χ at its own maximum for $q = 2, 4,$ and 10 .